PAPER

Optimized loading of Pt single atoms from platinic acid solution and the sweet spot for activity

Sutapa Dey, [ID] [a,b] Hyesung Kim,[a] Xin Zhou[a] and Patrik Schmuki [ID] *[a,b]

In recent years, platinum single atoms (SAs) have emerged as exceptionally efficient co-catalysts for photocatalytic hydrogen (H_2) evolution. In the present work, we systematically investigate the solution parameters that govern the deposition of Pt SAs from dilute H_2PtCl_6 precursors onto well-defined sputtered anatase TiO_2 thin films and evaluate the effect on photocatalytic H_2 evolution. We show that both precursor concentration and solution composition critically determine the oxidation state, dispersion, and reactivity of surface-bound Pt species. Ultra-dilute, additive-free solutions (0.001–0.005 mM) enable strong electrostatic adsorption (SEA) and aquation-assisted anchoring of isolated Pt^{2+} atoms, leading to atomically dispersed Pt–O–Ti surface motifs with maximal H_2 evolution per Pt. In contrast, increased ionic strength or unfavorable speciation caused by higher concentration or pH adjustment induces non-selective uptake, formation of Pt(IV)-rich 2D rafts, and diminished catalytic performance. Overall, we show that the placement and photocatalytic activity of Pt SAs are dictated by the pre-reaction deposition chemistry. From a practical view, this study defines a narrow yet actionable parameter window for scalable, efficient SA co-catalyst decoration and establishes the mechanistic basis for performance optimization *via* precursor-chemistry design.

1. Introduction

In recent years, supported single atoms (SAs) have attracted significant attention in various research domains, including heterogeneous catalysis,[1–4] electrocatalysis,[5–8] and most importantly, in photocatalytic processes such as water splitting,[9] waste degradation,[10] and CO_2 reduction.[11] In typical photocatalytic systems, upon illumination with photons exceeding a semiconductor's band gap energy, photogenerated charge carriers (electrons and holes) are generated that can migrate to the surface and drive redox reactions in the surrounding environment, such as the generation of H_2 from water or aqueous solutions. One of the most crucial steps in this process is the efficient transfer of photoexcited electrons from the conduction band of the semiconductor to H^+ or water molecules.[12,13] However, this electron transfer often faces kinetic limitations and thus requires the assistance of co-catalysts, specifically noble metals such as Pt, Pd, or Rh, which are well established to enhance the H_2 production.[12,14,15] Conventionally, these co-catalysts are attached onto semiconductor surfaces in the form of nanoparticles (NPs), typi-

cally a few nanometers in size.[16,17] In efforts to reduce the consumption of costly noble metals while maintaining high catalytic efficiency, much research has focused on optimizing both the size and loading of the co-catalyst.[18–20] The downscaling from nanoparticles to SAs has emerged as a significant advancement in this context, offering a dramatically increased surface-to-volume ratio, providing more active sites, and the potential for enhanced reactivity.[21] This is evident from several studies on photocatalytic performances of SAs co-catalysts supported on oxide semiconductors, particularly, on Pt SAs over TiO_2 supports,[14,22,23] which is the most extensively exploited photocatalyst, over the past few decades. A most promising approach for Pt SA decoration on TiO_2 is reactive deposition based on reductive anchoring of SAs from dilute hexachloroplatinic (IV) acid (H_2PtCl_6) solution, providing SA co-catalyst loading without any thermal post-deposition treatment.[24,25] Despite a number of studies using this approach for Pt SA deposition and elaborating consequent co-catalysts effects, a comprehensive and systematic investigation of the Pt precursor parameters on the resulting loading and the impact on the photocatalytic activity remains largely open. Therefore, the present work aims at identifying critical factors when using reactive deposition from H_2PtCl_6 solutions to decorate Pt SAs co-catalysts on a well-defined titania substrate – that is, DC sputter-deposited anatase thin films.

In many previous studies, single atoms (SAs) have been deposited onto TiO_2, specifically on various nanostructures such as nanotubes,[26–28] nanoflakes,[29,30] and powders,[23,31] primarily

[a]Department of Materials Science WW4-LKO, Friedrich-Alexander-University of Erlangen-Nuremberg, Martensstrasse 7, 91058 Erlangen, Germany. E-mail: schmuki@ww.uni-erlangen.de
[b]Regional Centre of Advanced Technologies and Materials, Czech Advanced Technology and Research Institute (CATRIN), Palacký University, Olomouc 78371, Czech Republic

to take advantage of the high surface area, which can enhance overall catalytic performance. In contrast to these approaches, our work utilizes TEM-transparent TiO$_2$ sputter-deposited substrates. These flat, compact films offer a well-defined geometry that simplifies illumination and characterization processes (XPS, TEM), allowing for precise evaluation of SA loading, spatial distribution, as well as their catalytic activity for photocatalytic H$_2$ generation under controlled illumination conditions.

These thin film anatase layers are then decorated using different concentrations of H$_2$PtCl$_6$ precursor in an aqueous medium (and under different pH-adjustment conditions) to systematically investigate the effect of precursor concentration and deposition conditions on Pt SA co-catalyst loading, and finally, to evaluate the effect of different Pt loading (conditions) on photocatalytic H$_2$ generation.

The results show that the deposition of Pt SAs from H$_2$PtCl$_6$ solutions is strongly dependent on precursor concentration, pH and conductivity of the solution. At low precursor concentrations, Pt is stabilized as isolated SAs, while under specific conditions, partial aggregation into less reactive nm-sized two-dimensional (2D) rafts can occur due to unfavorable solution speciation.

2. Experimental section

2.1 Fabrication of TiO$_2$ film on FTO substrate

TiO$_2$ films were fabricated following a procedure reported previously.[32] Briefly, TiO$_2$ thin films were deposited on cleaned FTO substrates by reactive DC magnetron sputtering. Before deposition, the Ti target was pre-conditioned in an argon atmosphere to remove surface oxides. A thin Ti interlayer was first applied to the FTO, followed by TiO$_2$ deposition under controlled Ar/O$_2$ flow and pressure conditions, with the substrate holder rotated to ensure uniform growth. Films were deposited at room temperature using 500 W sputtering power, with ~200 nm thickness adjusted by deposition time, and subsequently annealed in air at 450 °C for 1 h – these films were used for photocatalytic testing and surface analyses. In addition, ultrathin TiO$_2$ layers (~20 nm) were prepared using the same DC sputter conditions on TEM grids – these were used for HAADF-STEM and TEM-EDX analyses. These 20 nm films provide electron transparency for high-resolution HAADF-STEM and EDX analyses, allowing direct imaging and compositional mapping of atomically dispersed Pt species. These films were fabricated on a commercial Si/SiO$_2$ TEM grid with photolithographically defined 50 × 50 μm windows.

2.2 Pt SAs deposition on TiO$_2$ layers

In a standard SAs deposition process, aqueous solutions of H$_2$PtCl$_6$·6H$_2$O (Metakem, Germany) were prepared at different concentrations (0.0002, 0.001, 0.005, 0.05, 0.01, 1, 2, 5, or 10 mM), using ultrapure deionized water in a quartz cell. These prepared solutions were purged with argon gas for

15 min to remove dissolved oxygen. Subsequently, TiO$_2$ films deposited on FTO substrates were submerged in the precursor solutions. The reaction cells were properly sealed and covered to avoid any interaction with light, and kept for 1 h. After 1 h, the samples were thoroughly rinsed with deionized water and finally dried under a nitrogen flow.

2.3 Characterization

The surface and cross-section morphologies of Pt-TiO$_2$ samples were investigated by field-emission scanning electron microscopy (FE-SEM, S-4800, Hitachi). High-angle annular dark-field scanning transmission electron microscopy (HAADF-STEM) and Energy Dispersive X-Ray Spectroscopy (EDS) mapping were performed using a high-resolution transmission electron microscope (HRTEM, FEI Titan G2 60–300). The chemical states and composition of samples were analyzed by X-ray photoelectron spectroscopy (XPS, PHI 5600). The XPS spectral deconvolution was carried out using MultiPak software, and all XPS spectra were aligned by a binding energy of Ti 2p (458.5 eV).

2.4 Photocatalytic H$_2$ evolution

The photocatalytic H$_2$ evolution activity of TiO$_2$ layers loaded with Pt SAs was assessed under ultraviolet (UV) light irradiation. The experiments were conducted using a quartz reactor containing 10 mL of an aqueous solution with 50% methanol as a hole scavenger. Prior to illumination, the system was purged with argon gas for 15 min to remove dissolved oxygen. The reactor was then sealed and exposed to 365 nm LED light with a power density of 65 mW cm^{-2} for a predetermined period. Hydrogen production was monitored at set time intervals using a gas chromatograph instrument (GCMS-QO2010SE, SHIMADZU) equipped with a thermal conductivity detector (TCD).

3. Results and discussion

In a first set of experiments, Pt SAs were decorated on the anatase TiO$_2$ layers using immersion in a 0.005 mM H$_2$PtCl$_6$ precursor solution, as described in the Experimental section. High-resolution top-view and cross-sectional SEM images of the TiO$_2$ surface after Pt deposition are shown in Fig. 1(a) and (b), respectively. As expected, no deposition of particles or agglomeration is visible. These layers are ~200 nm thick and were later used further for photocatalytic experiments. On the 20 nm thick "sister" sample, to detect Pt SAs on the TiO$_2$ layers, high-angle annular dark-field scanning transmission electron microscopy (HAADF-STEM) was utilized. Fig. 1(c) shows an SEM image of the TEM grid, and Fig. 1(d) schematically illustrates the samples used for TEM. Fig. 1(e) presents a HAADF-STEM image of the TiO$_2$ layer after Pt SA deposition from the 0.005 mM H$_2$PtCl$_6$ solution. The image and the corresponding EDX mapping (Fig. S1) distinctly reveal that Pt SAs are well-dispersed and uniformly distributed across a TiO$_2$ substrate. The lattice spacing of 0.35 nm corresponds to the
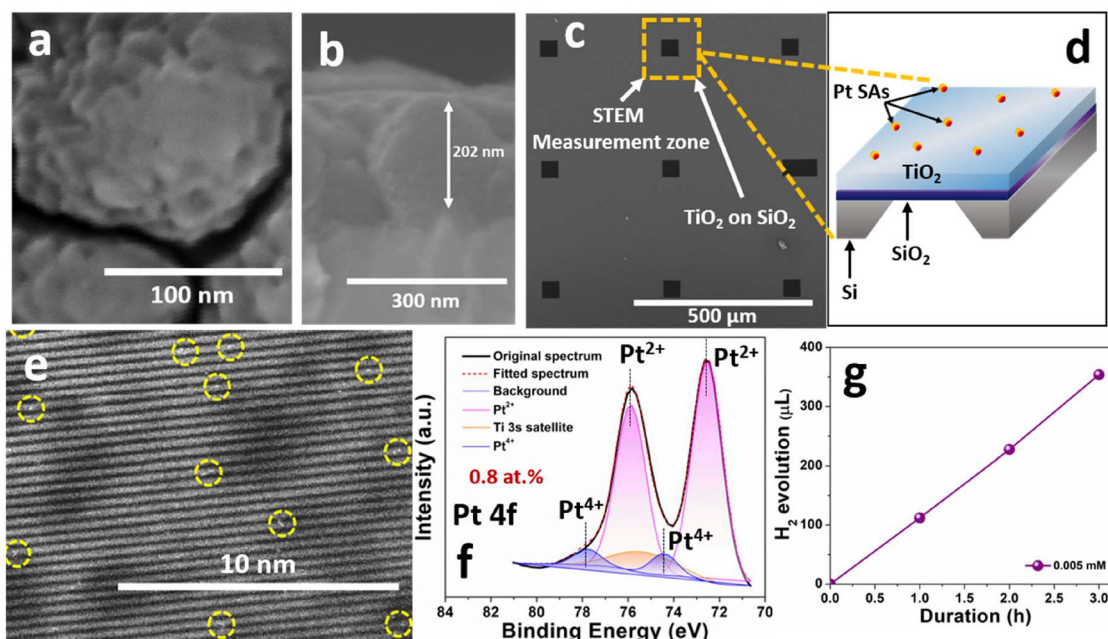
Fig. 1 (a) Top-view and (b) cross-sectional SEM images of Pt SAs decorated TiO$_2$ layers from H$_2$PtCl$_6$ (0.005 mM) solutions on FTO substrate, (c) SEM image of Pt SAs loaded 20 nm TiO$_2$ deposited onto the Si/SiO$_2$ TEM window, (d) schematic drawing of the layer on the TEM grid, (e) HAADF-STEM image, (f) XPS spectra of Pt 4f, and (g) H$_2$ evolution *vs.* duration from the Pt SAs decorated TiO$_2$ layer deposited using 0.005 mM H$_2$PtCl$_6$.

(101) planes of anatase. The surface density of Pt SAs was evaluated from several STEM images at a level of $\sim 7.9 \times 10^4$ μm^{-2}. Further, neither from STEM, SEM nor the TEM-EDX, any Pt SA agglomeration is visible on the surface. The XPS Pt 4f spectrum from the surface of the Pt SAs loaded TiO$_2$ layer from 0.005 mM H$_2$PtCl$_6$ solution is presented in Fig. 1(f). The spectrum evidences the presence of Pt with an intense doublet of Pt 4f$_{7/2}$ and Pt 4f$_{5/2}$ at the respective positions of 72.5 eV and 75.9 eV, which corresponds to the typical speciation of Pt SAs coordinated with an oxide in a (+2) state. Quantitative analysis of the spectrum indicates a total Pt concentration of 0.8 at%, of which 0.65 at% corresponds to surface-anchored Pt^{2+} species. It is important to note that there is a significant difference in the position of these peaks from the metallic Pt^0 (in nanoparticles), which are usually located for the Pt 4f doublet at ~ 70.9 eV and ~ 74.1 eV, respectively (an example is given in Fig. S2(a)). Note that in Fig. 1(f), small contributions are also observed at 74.4 eV and 77.8 eV, which correspond to Pt^{4+} – likely traces of adsorbed H$_2$PtCl$_6$ precursor. Notably, the XPS spectrum (Fig. S3(b)) reveals a negligible amount of Cl.

These layers, as in Fig. 1(a) and (b), were then tested for photocatalytic H$_2$ evolution using a 365 nm LED (65 mW cm^{-2}) as a light source. The samples were illuminated in 10 mL of an aqueous solution containing 50% methanol as a hole scavenger, and evolving H$_2$ was detected using gas chromatography (GC), as described in the Experimental section. Fig. 1(g) shows the produced H$_2$ volume over illumination time. From the linear slope of the data, an H$_2$ evolution rate of ~ 117.9 μL h^{-1} was determined.

From this starting point, we then screened critical factors in the reactive deposition process and their correlation with Pt deposition amount, speciation and the resulting photocatalytic performance. In a first assessment, we used different concentrations of the H$_2$PtCl$_6$ precursor in the range from 0.0002 mM to 10 mM, where the precursor was simply dissolved in DI water and no further solution adjustments (pH, ionic strength) were performed. All samples were then characterized by SEM and XPS. Fig. 2(a) gives the Pt loading on the TiO$_2$ surface obtained for the different concentrations of H$_2$PtCl$_6$. The result shows that initially, the Pt loading increases with increasing H$_2$PtCl$_6$ concentration in the precursor solution and reaches a highest loading amount of 5.4 at% from the 0.1 mM Pt precursor solution. However, for higher concentrations of H$_2$PtCl$_6$ beyond 0.1 mM, the loading amount of Pt gradually decreases. To investigate the activity of the Pt deposited on the TiO$_2$ surfaces, the photocatalytic H$_2$ evolution was evaluated for all samples (Fig. 2(b)), and Fig. 2(c) plots the photocatalytically generated H$_2$ rate (determined from Fig. 2(b) using the volume of H$_2$ produced over 3 h normalized with time) for the different concentrations of Pt precursor. In terms of precursor concentration, a maximum Pt loading is achieved for a Pt loading of ~ 5.4 at% on the TiO$_2$ surface from the 0.1 mM H$_2$PtCl$_6$ solution. Beyond this point, further increase in the H$_2$PtCl$_6$ concentration in the solution leads to lower Pt loading, and the H$_2$ evolution rate deteriorates. Overall, the activity shows an even maximum distribution ("Bell-type") curve except for two distinct data points at 0.1 and 0.05 mM. These two samples show, in XPS, SEM, and STEM, unusual findings. SEM images reveal a
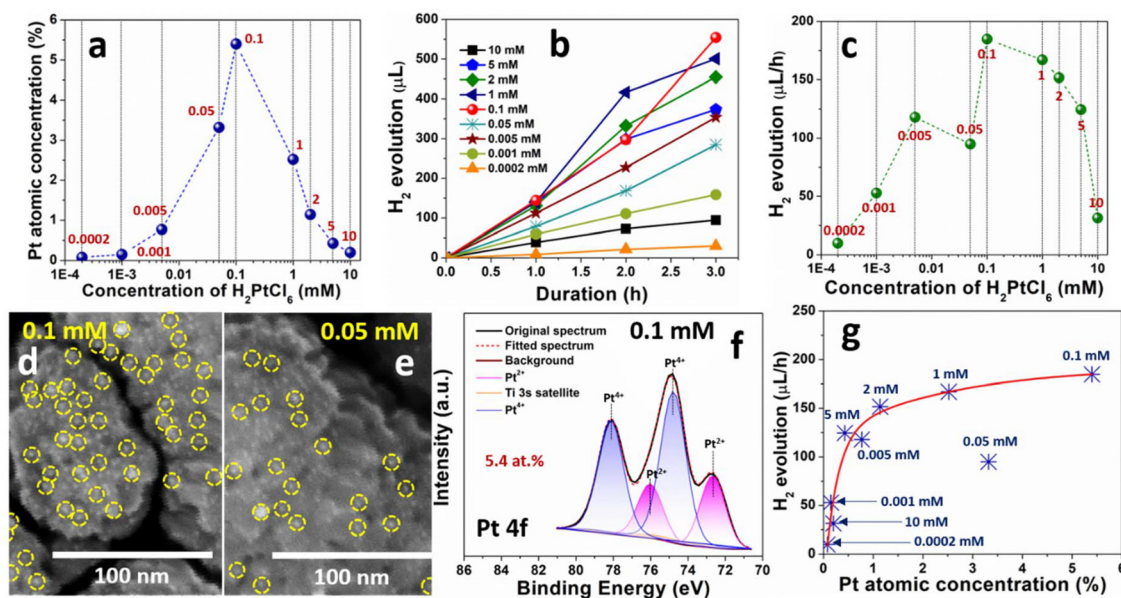
Fig. 2 (a) Pt loading *vs.* H_2PtCl_6 concentration, (b) H_2 evolution *vs.* duration using different concentrations of H_2PtCl_6, (c) H_2 evolution rate *vs.* concentration of H_2PtCl_6 in solution from the Pt SAs decorated TiO_2 layer, SEM images of Pt SAs decorated TiO_2 layers from (d) 0.1 mM and (e) 0.05 mM H_2PtCl_6 solutions, (f) XPS spectra of Pt 4f from the Pt SAs decorated TiO_2 layer deposited using 0.1 mM H_2PtCl_6, and (g) H_2 evolution *vs.* Pt loading amount from different concentrations of H_2PtCl_6. A few examples of the SA assembly/2D rafts are marked with yellow circles in (d) and (e).

similar microscopic observation for all samples in the entire concentration range from 0.0002 mM to 10 mM, that is, no detectable deposition of particles or clusters, except for the samples prepared at 0.1 mM and 0.05 mM, respectively, where clear particle deposition is observed (Fig. 2(d) and (e)). This is confirmed in the HAADF-STEM, where, except for Pt SAs, also 2D rafts can be seen (Fig. S4). The HAADF-STEM images clearly show that the majority of Pt is in the SA form with a surface density of $\sim 1.7 \times 10^5$ μm^{-2}. However, clearly 2D rafts ($\sim 5.7 \times 10^4$ μm^{-2}) are also observed. For all samples, the XPS spectra (Fig. S3(a)) show peak positions corresponding to Pt^{2+} oxidation states, reflecting the presence of Pt in SA form. However, for the layers Pt deposited in the range from 0.05 mM to 1 mM H_2PtCl_6, a strong doublet peak is also observed at ~ 74.8 eV (Pt $4f_{7/2}$) and ~ 78.1 eV (Pt $4f_{5/2}$), indicating the presence of significant amounts of Pt^{4+}. Since there is hardly any Cl^- species detectable (Fig. S3(b)) nor any metallic species, and an additional contribution from adsorbed oxygen species is observed in ~ 531–532 eV range in the O 1s spectra (Fig. S3(c)), it can be concluded that the H_2PtCl_6 in this case reacted to a fully hydrolysed Pt^{4+} species, *i.e.*, a hydroxy- or aquo-species that agglomerated on the TiO_2 surface. Table 1 presents the atomic concentration of Pt^{2+} and Pt^{4+} oxidation states for the Pt SAs loaded TiO_2 layers from different concentrations of the precursor solution. From the HAADF-STEM, even the larger assemblies still consist of 2D rafts rather than 3D particles. All in all, this suggests that coalescence of complexes (likely non-charged Pt(IV) species in solution) has taken place for the two critical concentrations. If the XPS Pt loading data are used to plot the photocatalytic H_2 evolution activity with respect to the Pt

Table 1 Atomic concentration of Pt^{2+} and Pt^{4+} for different concentrations of H_2PtCl_6

Concentration of H_2PtCl_6	Pt^{2+} at%	Pt^{4+} at%
0.0002 mM	0.06	0.01
0.001 mM	0.13	0.01
0.005 mM	0.65	0.05
0.05 mM	1.54	1.72
0.1 mM	1.63	3.68
1 mM	1.14	1.31
2 mM	0.79	0.31
5 mM	0.37	0.04
10 mM	0.15	0.04

loading amount (Fig. 2(g)), overall, an increase in the Pt loading amount enhances the H_2 generation activity, but only up to a certain threshold. For Pt surface concentrations up to ~ 0.2–0.5 at%, the Pt loading strongly affects the H_2 evolution activity; for higher loadings, the effect saturates. Therefore, the results suggest that an optimal concentration of deposited Pt for achieving maximum Pt activity is ~ 0.2–0.5 at%, beyond which the Pt loading does not increase the activity, *i.e.*, leading to Pt material waste. Remarkably, this loading can be achieved already with very dilute precursor solutions (0.001 mM– 0.005 mM), indicating that a maximum beneficial effect is achieved in this very low concentration range in terms of deposition efficiency as well as reactivity of the deposited species.

To evaluate the origin of the Pt loading distribution as a function of precursor concentration (in Fig. 2(a)) and its compliance with a basic strong electrostatic adsorption (SEA)

concept,[24] the pH and conductivity of the precursor solutions were determined (Fig. 3(a)). It is evident that, as expected, with increasing concentration of the H_2PtCl_6 precursor in the aqueous medium, the pH of solutions gradually decreases, from ~5.5 to 2.0, while the conductivity of the solutions increases accordingly from ~0.01 to 7.5 mS cm^{-1}. Considering the point of zero charge (PZC) for anatase is in the range of 5.5–6.5,[33] all H_2PtCl_6 solutions should be able to provide electrostatically absorbable species as long as their hydrolysis leads to a negatively charged species (e.g., $[PtCl_6]^{2-}$, $[PtCl_5(OH)]^{2-}$, $[PtCl_4(OH)_2]^{2-}$, etc.). In general, the lower the pH, the higher the positive charge on the TiO_2 surface, but the speciation of the hydrolyzed precursor ($[PtCl_x(H_2O)_y]^{n-}$) may be less favorable for adsorption.[33] It is reported that partial hydrolysis of $[PtCl_6]^{2-}$ increases the possibility of adsorption and subsequent anchoring of Pt species.[33] At lower pH, near ~2.6, partial hydrolysis of $[PtCl_6]^{2-}$ occurs with complexes containing 2–3 Pt–O bonds and a few Pt–Cl bonds,[34] while for higher pH, the hydrolysis increases OH coordination (mainly OH and H_2O become dominant ligands).[35] The speciation of Pt to partially hydrolyzed species, i.e., mixed Cl and O coordinates,

reaches its peak at pH ~ 3 to 4, which often makes this range ideal for partial hydrolysis-enabled adsorption and complexation via electrostatic and possible coordination mechanisms.[34,36] This is in line with our results, i.e., the highest Pt loading from the 0.1 mM (pH ~ 3.5) H_2PtCl_6 solution and the highest photocatalytic H_2 evolution activity of the TiO_2 layer. Such behavior is consistent with SEA, where controlled precursor hydrolysis and charge complementarity guide preferential deposition of metal species on oxide supports. However, in this pH range (~3.5 to ~4.5), speciation also leads to neutrally charged complexes. Particularly, the neutral species, $[PtCl_4(H_2O)_2]^0$, dominates near pH ~ 4,[36] which reduces the driving force for coulombic adsorption since electrostatic attraction to the positively charged TiO_2 surface is absent. In fact, the odd point in Fig. 2(c) for 0.05 mM corresponds to pH ~ 4.0 and thus the presence of abundant zero-charged complexes. Due to the lack of repulsive charge on the complexes, under these conditions, these Pt^{4+} species are prone to uncontrolled deposition and aggregation rather than well-dispersed anchoring, which compromises the formation of tight bonds and isolated SAs. Below pH ~ 2, it is more likely
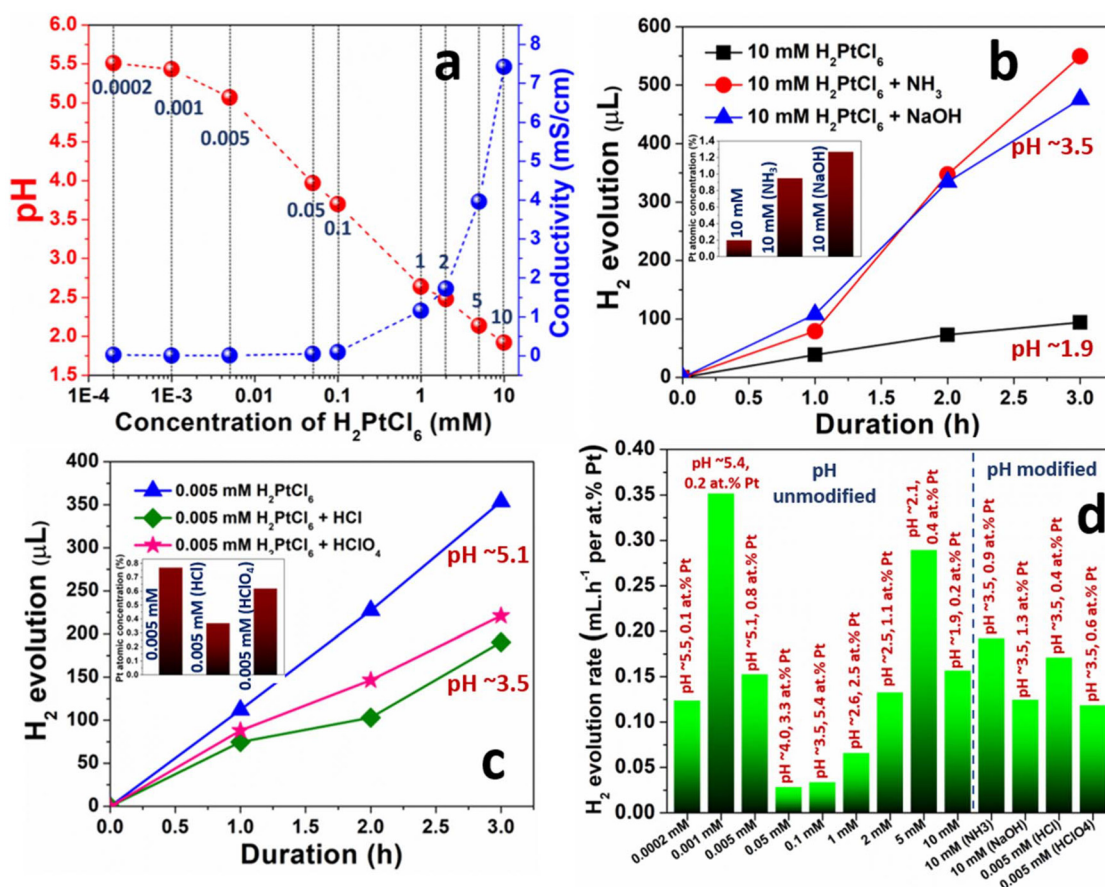

Fig. 3 (a) pH and conductivity vs. concentration of H_2PtCl_6. (b) H_2 evolution vs. duration from the Pt SAs decorated TiO_2 layer from 10 mM H_2PtCl_6 with modified pH using NH_3 and NaOH. (c) H_2 evolution vs. duration from the Pt SAs decorated TiO_2 layer from 0.005 mM H_2PtCl_6 with modified pH using HCl and $HClO_4$. (d) H_2 evolution normalized to Pt at% comparison chart for Pt SAs loaded TiO_2 layers deposited from various H_2PtCl_6 solutions with adjusted pH.

to observe a speciation in the fully chlorinated form $[PtCl_6]^{2-}$ as hydrolysis is strongly suppressed. In such cases, the combination of limited hydrolysis and high ionic strength diminishes adsorption efficiency, and the process may even become dominated by ionic shielding effects rather than direct surface–species interaction, which leads to very low Pt loading.[36] Importantly, Pt loading exhibits an upper limit under the studied deposition conditions. Although isolated cases show relatively high loadings, the uptake of Pt SAs saturates at approximately 1.2 at% Pt. At the higher precursor concentrations, particularly at pH < 2, adsorption may be controlled by ionic screening effects (of the surface charge), i.e., the dominant factor is the ionic strength of the precursor solution.[36] Furthermore, the variation in Pt oxidation states (Table 1) primarily reflects the extent of precursor–surface interaction. The catalytically active Pt^{2+} species forms through surface-mediated reduction during deposition, where partially hydrolyzed Pt(IV) complexes are reduced via charge transfer with Ti^{3+} sites to yield stable Pt–O–Ti linkages, as previously reported.[37,38] Minor Pt^{4+} contributions at most concentrations likely arise from residual Pt(IV) complex adsorption. At intermediate precursor concentrations (~0.05–0.1 mM, pH ~ 3.5–4.0), neutral hydrolyzed Pt(IV) species (partially agglomerated) can attach non-selectively, causing partial aggregation and increased Pt^{4+} content. Their accumulation explains the bell-shaped trend in Pt loading and H_2 evolution, as these aggregated Pt(IV)-rich domains are largely inactive compared to isolated Pt^{2+} sites. Additionally, at higher precursor concentration (low pH), the limited number of high-affinity anchoring sites on the TiO_2 surface may play a limiting role in the saturation behavior of the Pt loading. Once high-affinity sites are occupied, further deposition occurs on less reactive or weakly coordinated regions, leading to a decline in intrinsic activity per Pt atom.

Based on these findings, in further experiments, we adjusted the pH of the precursor solution to an optimized speciation region that is pH ~ 3.5. Solutions with pH < 3.5 were adjusted using NaOH and NH_3, respectively, and solutions with pH > 3.5 using HCl and $HClO_4$, respectively. Fig. 3(b) shows the Pt loading and the resulting photocatalytic H_2 evolution for 10 mM H_2PtCl_6 solution with an adjusted pH at ~3.5 using NH_3 and NaOH, respectively. Compared with the non-pH corrected sample (0.2 at% Pt), XPS analysis for these (Fig. S5(a)) reveals an increase in the Pt loading onto the TiO_2 layer surface using NH_3 (to 0.9 at%) and NaOH (to 1.3 at%) for the modified H_2PtCl_6 solution, but still maintaining full SA signatures. The corresponding SEM images of the Pt SA decorated TiO_2 layers from the pH-modified (pH ~ 3.5) 10 mM precursor solutions (NH_3 in Fig. S6(a) and NaOH in Fig. S6(b)) show the absence of any Pt agglomerates on the surfaces. Evidently, the photocatalytic H_2 evolution increased by a factor of ~6 and ~5, after adjusting the pH of the 10 mM H_2PtCl_6 solution using NH_3 and NaOH, respectively, demonstrating the strong influence of pH on the adsorption behavior of the Pt species. More importantly, with a very low Pt loading (~1 at%) in comparison to the 0.1 mM H_2PtCl_6 solution (~5.4 at%), a

maximum photocatalytic H_2 evolution activity, equivalent to that of the 0.1 mM H_2PtCl_6 solution, was obtained from the pH-modified (pH ~ 3.5) 10 mM precursor solutions. These results confirm that for the adsorption of complexes from H_2PtCl_6 onto TiO_2, an optimum pH is beneficial. Under these conditions, the pH effect dominates the process, strongly influencing the surface–complex interaction and thereby controlling the extent of adsorption. Consequently, with optimized pH adjustment using NH_3 and NaOH, also a very high photocatalytic H_2 evolution activity was achieved (comparable to or even higher than the best non-pH-adjusted case).

In a control experiment, we adjusted the pH of the deposition solution using HCl and $HClO_4$, respectively, with a 0.005 mM H_2PtCl_6 solution (pH ~ 5.1) and adjusted the pH value to ~3.5. Unlike the case with the 10 mM solutions, here the pH adjustment did not enhance the Pt uptake or the photocatalytic activity. Instead, a clear reduction in Pt loading was observed, accompanied by a corresponding decrease in photocatalytic H_2 evolution performance. Fig. 3(c) shows the results of normalized Pt loading and H_2 generation. In this case, a detrimental effect of the pH adjustment is detected: less Pt is deposited, and consequently, less activity is achieved.

From above discussion, the deterioration in the photocatalytic performance can be ascribed to the combined effects of ionic strength and counter-ion chemistry introduced by the use of strong acids such as HCl and $HClO_4$. Specifically, the high concentration of counter-ions (Cl^- or ClO_4^-) leads to shielding at the TiO_2/solution interface that reduces the effective interaction between the negatively charged Pt complexes and the TiO_2 surface. Furthermore, the chloride ions play a reactive role in the hydrolysis and speciation pathways of H_2PtCl_6, i.e., the speciation of the Pt complexes in solution and the equilibrium with adsorbed species on the TiO_2 surface.

Please note, the conductivity of the solution also increases from ~0.01 mS cm^{-1} to ~0.36 mS cm^{-1} (for HCl) and to ~0.46 mS cm^{-1} (for $HClO_4$) upon the introduction of the strong acids, reflecting a stronger coulombic shielding of the surface. In contrast, the use of bases such as NH_3 and NaOH for pH adjustment promoted not only a more favorable speciation, but also did not strongly affect the conductivity, i.e., ~2.62 mS cm^{-1} (for NH_3) and ~2.44 mS cm^{-1} (for NaOH) relative to the unmodified 10 mM solution (~7.42 mS cm^{-1}).

These results demonstrate the overlap of factors that dictate the uptake and activity of Pt on a TiO_2 surface exposed to H_2PtCl_6.

The photocatalytic H_2 evolution performances from the Pt SA loaded TiO_2 layers deposited from various H_2PtCl_6 solutions with different concentrations and pH are presented in Fig. 3(d), which demonstrates the strong and interconnected effect of the parameters, such as precursor concentration, solution pH, ionic strength, and counter-ion chemistry of the Pt precursor solution in controlling Pt adsorption, dispersion, and ultimately the photocatalytic activity. Importantly, the plot reveals an efficient photocatalytic activity from the dilute precursor solutions for the range of 0.001 mM–0.005 mM concen-

trations, suggesting the high activity with minimal utilization of Pt.

This interplay between precursor speciation, surface adsorption, and solution conductivity provides a more complete mechanistic understanding of the observed trends.

In summary, the observed trends reflect a surface electrostatic adsorption (SEA)-driven and aquation-assisted grafting process that defines the pre-reaction state of Pt. In ultra-dilute, additive-free H_2PtCl_6 solutions, anionic hydrolyzed Pt(IV) species (e.g., $[PtCl_2(OH)_4]^{2-}$ and other partially aquated forms) are accordingly selectively attracted to positively charged Ti–OH_2^+ sites on the sputtered TiO_2 surface. The low ionic strength preserves a long Debye length, restricting uptake to spatially separated, high-affinity or highly reactive surface sites. In particular, both solution-phase hydrolysis and surface-mediated reactions play crucial roles in determining the final activity of the deposited Pt; however, their contributions differ in terms of timing and extent. The solution-phase speciation, controlled by precursor concentration, pH, and ionic strength, primarily dictates the coordination environment of Pt complexes available for adsorption. Within the optimal pH range ($\sim$3.5–4.0), partially hydrolyzed Pt(IV) species predominate and can readily interact with the positively charged TiO_2 surface.[35,36] Once adsorbed, surface-mediated ligand exchange and charge-transfer processes promote partial reduction of Pt(IV) to Pt^{2+}, which becomes stabilized through Pt–O–Ti bond formation. Therefore, while surface reactions define the final stabilization of Pt^{2+} on TiO_2, the solution-phase hydrolysis largely governs the precursor-state of the Pt species available for deposition. Notably, XPS confirms that the anchored species are present in a reduced Pt^{2+} state prior to photocatalytic operation, indicating that the speciation/adsorption/reactive deposition sequence determines both the oxidation state and dispersion. An overall optimum is present at a pH of 3.5 solution with an ionic strength as low as possible. Increasing precursor concentration or modifying pH perturbs this pathway: high ionic strength and altered speciation (e.g., the occurrence of zero-charged complexes) reduce site selectivity, leading to aggregation and the formation of large (SEM visible >1 nm) 2D rafts. Consequently, various factors govern the activity per Pt atom. In general, maintaining dilute, excess precursor-free but pH-optimized conditions is key to provide reproducible Pt decoration in order to access the highly efficient SA regime.

even small changes in ionic strength or speciation—such as those induced by pH adjustment—disrupt selective anchoring and promote the formation of Pt(IV)-rich surface rafts or clusters before any catalytic reaction takes place. These aggregated forms lower the intrinsic activity per Pt and cannot be rescued by subsequent reduction or illumination. XPS and STEM data demonstrate that under optimized conditions, the Pt remains atomically dispersed and in the +2 oxidation state prior to catalysis. Taken together, our results demonstrate that performance is controlled not by total Pt content but by the solution-mediated anchoring step, which dictates the local coordination environment and surface dispersion of Pt. These insights establish a clear and actionable protocol—ultra-dilute precursor, unmodified pH, and low ionic strength—for preparing supported Pt single-atom catalysts with high reproducibility and superior catalytic performance.

Author contributions

Dr Sutapa Dey: investigation, writing – original draft, review & editing, validation, visualization. Dr Hyesung Kim: writing – review & editing, investigation, visualization. Dr Xin Zhou: investigation. Prof. Patrik Schmuki: conceptualization, supervision, project administration, funding acquisition, writing – review & editing.

Conflicts of interest

The authors declare that there is no conflict of interest.

Data availability

The data that support the findings of this study are available from the corresponding author upon reasonable request.

Supplementary information (SI) is available. See DOI: https://doi.org/10.1039/d5nr03976b.

4. Conclusions

This study identifies and isolates the solution chemistry conditions required for reproducible formation of high-efficiency Pt single-atom co-catalysts on sputtered TiO_2 thin films. Using a structurally defined and morphologically flat substrate, we show that deposition from highly dilute, additive-free aqueous H_2PtCl_6 selectively yields isolated Pt^{2+} species with maximal photocatalytic H_2 evolution rates per Pt. Systematic variation of precursor concentration and solution composition reveals that

Acknowledgements

References

1 D. Liu, Q. He, S. Ding and L. Song, *Adv. Energy Mater.*, 2020, **10**, 2001482.

2 S. Mitchell and J. Pérez-Ramírez, *Nat. Commun.*, 2020, **11**, 4302.

3 X. Li, X. Yang, Y. Huang, T. Zhang and B. Liu, *Adv. Mater.*, 2019, **31**, 1902031.

4 H. Zhang, G. Liu, L. Shi and J. Ye, *Adv. Energy Mater.*, 2018, **8**, 1–24.

5 J. Su, R. Ge, Y. Dong, F. Hao and L. Chen, *J. Mater. Chem. A*, 2018, **6**, 14025–14042.

6 Q. Zhang and J. Guan, *Adv. Funct. Mater.*, 2020, **30**, 2000768.

7 W. Zang, Z. Kou, S. J. Pennycook and J. Wang, *Adv. Energy Mater.*, 2020, **10**, 1903181.

8 C. Zhu, S. Fu, Q. Shi, D. Du and Y. Lin, *Angew. Chem., Int. Ed.*, 2017, **56**, 13944–13960.

9 Q. Zhang and J. Guan, *Sol. RRL*, 2020, **4**, 2000283.

10 H. Zeng, Y. Chen, J. Xu, J. Li, D. Li and J. Zhang, *J. Environ. Chem. Eng.*, 2023, **11**, 110681.

11 Z. Shang, X. Feng, G. Chen, R. Qin and Y. Han, *Small*, 2023, **19**, 2304975.

12 X. Chen, S. Shen, L. Guo and S. S. Mao, *Chem. Rev.*, 2010, **110**, 6503–6570.

13 S. Dey and S. C. Roy, *J. Alloys Compd.*, 2021, **881**, 160481.

14 S. M. Wu and P. Schmuki, *Adv. Mater.*, 2024, **37**, 2414889.

15 B. Liu, Z. Hu, Z. Li, X. Tan, J. Ye and T. Yu, *Nat. Commun.*, 2025, **16**, 6014.

16 A. Kumar, P. Choudhary, A. Kumar, P. H. C. Camargo and V. Krishnan, *Small*, 2022, **18**, 2101638.

17 D. Benz, K. M. Felter, J. Köser, J. Thöming, G. Mul, F. C. Grozema, H. T. Hintzen, M. T. Kreutzer and J. R. Van Ommen, *J. Phys. Chem. C*, 2020, **124**, 8269–8278.

18 J. Ma, X. Tan, Q. Zhang, Y. Wang, J. Zhang and L. Wang, *ACS Catal.*, 2021, **11**, 3352–3360.

19 I. Vamvasakis, B. Liu and G. S. Armatas, *Adv. Funct. Mater.*, 2016, **26**, 8062–8071.

20 C. Dong, C. Lian, S. Hu, Z. Deng, J. Gong, M. Li, H. Liu, M. Xing and J. Zhang, *Nat. Commun.*, 2018, **9**, 1252.

21 K. Maiti, S. Maiti, M. T. Curnan, H. J. Kim and J. W. Han, *Adv. Energy Mater.*, 2021, **11**, 2101670.

22 S. Qin, J. Will, H. Kim, N. Denisov, S. Carl, E. Spiecker and P. Schmuki, *ACS Energy Lett.*, 2023, **8**, 1209–1214.

23 S. Qin, N. Denisov, B. B. Sarma, I. Hwang, D. E. Doronkin, O. Tomanec, S. Kment and P. Schmuki, *Adv. Mater. Interfaces*, 2022, **9**, 2200808.

24 Y. Wang, S. Qin, N. Denisov, H. Kim, Z. Bad'ura, B. B. Sarma and P. Schmuki, *Adv. Mater.*, 2023, **35**, 2211814.

25 Y. Wang, N. Denisov, S. Qin, D. S. Gonçalves, H. Kim, B. B. Sarma and P. Schmuki, *Adv. Mater.*, 2024, **36**, 2400626.

26 I. Hwang, A. Mazare, J. Will, T. Yokosawa, E. Spiecker and P. Schmuki, *Adv. Funct. Mater.*, 2022, **32**, 2207849.

27 Z. Wu, I. Hwang, G. Cha, S. Qin, O. Tomanec, Z. Badura, S. Kment, R. Zboril and P. Schmuki, *Small*, 2022, **18**, 2104892.

28 X. Zhou, I. Hwang, O. Tomanec, D. Fehn, A. Mazare, R. Zboril, K. Meyer and P. Schmuki, *Adv. Funct. Mater.*, 2021, **31**, 2102843.

29 G. Cha, A. Mazare, I. Hwang, N. Denisov, J. Will, T. Yokosawa, Z. Badura, G. Zoppellaro, A. B. Tesler, E. Spiecker and P. Schmuki, *Electrochim. Acta*, 2022, **412**, 140129.

30 G. Cha, I. Hwang, S. Hejazi, A. S. Dobrota, I. A. Pašti, B. Osuagwu, H. Kim, J. Will, T. Yokosawa, Z. Badura, Š. Kment, S. Mohajernia, A. Mazare, N. V. Skorodumova, E. Spiecker and P. Schmuki, *iScience*, 2021, **24**, 102938.

31 S. Qin, N. Denisov, J. Will, J. Kolařík, E. Spiecker and P. Schmuki, *Sol. RRL*, 2022, **6**, 2101026.

32 H. Kim, Y. Wang, N. Denisov, Z. Wu, Š. Kment and P. Schmuki, *J. Mater. Sci.*, 2022, **57**, 12960–12970.

33 K. Wenderich and G. Mul, *Chem. Rev.*, 2016, **116**, 14587–14619.

34 Y. Zhao, L. Wang, A. Kochubei, W. Yang, H. Xu, Y. Luo, A. Baiker, J. Huang, Z. Wang and Y. Jiang, *J. Phys. Chem. Lett.*, 2021, **12**, 2536–2546.

35 W. A. Spieker, J. Liu, J. T. Miller, A. J. Kropf and J. R. Regalbuto, *Appl. Catal., A*, 2002, **232**, 219–235.

36 W. A. Spieker, J. Liu, X. Hao, J. T. Miller, A. J. Kropf and J. R. Regalbuto, *Appl. Catal., A*, 2003, **243**, 53–66.

37 S. M. Wu, I. Hwang, B. Osuagwu, J. Will, Z. Wu, B. B. Sarma, F. F. Pu, L. Y. Wang, Z. Badura, G. Zoppellaro, E. Spiecker and P. Schmuki, *ACS Catal.*, 2023, **13**, 33–41.

38 S. Qin, N. Denisov, H. Kim and P. Schmuki, *Angew. Chem., Int. Ed.*, 2024, **63**, e202316660.